PAPER

Assessment of phonon scattering-related mobility in β-Ga$_2$O$_3$

View the article online for updates and enhancements.

IOP ebooks™

Bringing you innovative digital publishing with leading voices to create your essential collection of books in STEM research.

Start exploring the collection - download the first chapter of every title for free.

Assessment of phonon scattering-related mobility in β-Ga$_2$O$_3$

A Parisini[1] , K Ghosh[2] , U Singisetti[2] and R Fornari[1]

[1] Dept. of Mathematical, Physical and Computer Sciences, University of Parma, Viale Area delle Scienze 7/A, I-43124 Parma, Italy
[2] Electrical Engineering Department, University at Buffalo, Buffalo, NY 14260, United States of America

E-mail: antonella.parisini@unipr.it

Abstract

The momentum scattering time for electron–phonon interaction in β-Ga$_2$O$_3$ was derived within the relaxation time approximation considering all infra-red active optical modes. A first principle calculation was applied to separately obtain the scattering rates due to polar and non-polar phonon–electron interactions, and then spherically averaged coupling coefficients for each polar optical mode were calculated. The method was tested to analyze, in the framework of the relaxation time approximation, transport data in semiconductors having different optical phonons. This approach can be reliably applied if the band may be considered as isotropic. Hall density and mobility curves were fitted simultaneously with the same parameters, after Hall-to-drift data conversion through a Hall scattering factor calculated self-consistently within the routine. In the theoretical mobility calculations, both polar and non-polar phonon interactions were considered besides impurity scattering. The Farvacque correction was included in the momentum scattering rate for electron interaction with the optical phonons, and its effect on mobility calculation is critically discussed. Hall transport data of β-Ga$_2$O$_3$ taken from the literature were fitted to test the approach, and good agreement between the experimental and calculated mobilities was obtained.

Keywords: oxide semiconductors, electronic transport in semiconductors, electron mobility, β-Ga$_2$O$_3$ single crystal

(Some figures may appear in colour only in the online journal)

Introduction

Gallium oxide (β-Ga$_2$O$_3$) is a wide band gap semiconductor that has attracted great interest for its demonstrated applications in fields such as power electronics, optoelectronics, photovoltaics, and gas sensors [1–8]. Materials growth and characterization, as well as prototype devices (especially Schottky diodes, UV photodetectors, FETs and MOSFETs) are the subject of numerous publications [9–12]. Understanding basic physical properties is important for both control of material properties and improvement of device performances. Transport properties are certainly those that mostly influence design and fabrication of high-performance devices. In the case of β-Ga$_2$O$_3$, modeling and investigation of transport parameters are however complicated by the low symmetry of the crystal (monoclinic, belonging to the space group C2/m), resulting in anisotropic optical, thermal and vibrational properties [13–16]. There is a large set of vibrational modes: 30 phonon branches, consisting of three acoustic modes and 27 optical modes. Among the latter, 12 modes are polar, IR active modes: eight of B$_u$ symmetry, four of A$_u$ symmetry; while ten of the residual 15 optical modes have A$_g$ symmetry and five B$_g$ symmetry [17, 18]. Despite the expected anisotropic conductive and magneto-conductive tensor of a monoclinic structure [19–21], the experimental and calculated electrical properties show nearly isotropic behavior [22, 23]. It is generally recognized that the bottom of the conduction band (CB), at the gamma point of the Brillouin zone, is essentially parabolic and spherical, with minor differences in the effective masses for the different k directions [24, 25]. The scattering mechanism anisotropy is also expected to be moderate, as demonstrated by mobility measurements in MOSFETs with different channel orientations for which the mobility was statistically contained within

10%–15% [26]. Theoretically, the mobility anisotropy of β-Ga$_2$O$_3$ was predicted to be within 30% for low-doped β-Ga$_2$O$_3$ [23]. On the other hand, at very high doping levels the ionized impurity scattering may also become anisotropic owing to the anisotropy of the dielectric tensor, with anisotropy estimated to be less than 40% [23]. These experimental and theoretical results imply that the diagonal elements of the conductivity (and resistivity) tensor are practically equal while the non-diagonal ones are negligible. This allows one to use the van der Pauw method for the measurement of the transport properties and to use the simplified expression of the Hall coefficient R_H, based on the analytical solution of the Boltzmann equation in the so-called relaxation time approximation (RTA) [19]. This means that: $R_H = r_H/ne$, where $r_H = \langle \tau^2 \rangle / \langle \tau^2 \rangle$, where r_H is the Hall scattering factor, τ the energy-dependent scattering time n the drift electron density and e the electronic charge [19, 27].

The literature on transport data of β-Ga$_2$O$_3$ includes Hall mobility and Hall electron density curves as a function of temperature [22, 28–32], doping level [22, 33, 34], or crystal orientation [25, 26]. First principle calculations have also been performed to clarify the dominant scattering mechanisms [23, 35] and other aspects of transport [36, 37].

A common finding of the latest theoretical computation is that the lattice mobility is controlled by optical phonons (OP), with a low energy of about 25–30 meV. The first principle calculations reported in [23, 35] suggested that the scattering with polar optical phonons (POP) strongly prevails on the electron–phonon interaction via deformation potential (DP), from acoustic (AC) and non-polar optical (NOP) phonons. On the other hand, considering the $T^{-1.5}$ temperature dependence of experimental mobility data, some of the present authors proposed a model according to which the mobility was essentially determined by NOP scattering [19]. The estimated NOP deformation potential had the character of averaged non-polar interactions by several phonons. In that work, the POP mobility has been attributed to a single effective optical phonon of high energy, considering the fact that electron–POP coupling increases with increasing LO phonon energy, as suggested by Liu *et al* [17]. However, accounting for anisotropy of the LO–TO splitting, Ghosh and Singisetti found that the POP B$_u$1 mode has the biggest coupling strength and thus a major impact on mobility at low-electric field and room temperature (RT) [35]. A very strong Froehlich interaction is also expected owing to a relatively high ionicity of the chemical bonds, as Ma *et al* [38] recently pointed out. These authors evaluated the intrinsic mobility by considering an effective momentum scattering time in RTA approach to account for the overall polar electron–phonon interactions. This again implies that just one effective single PO mode is considered in order to calculate the POP mobility, anyhow of lower energy (44 meV deduced from the fit of the experimental data).

The present work aims to calculate the total momentum scattering time for the polar interaction of optical phonons and electrons, by taking into account the multiplicity of the polar vibrational branches through the overlap of independent POP modes. A practical, reliable RTA routine able to calculate the total POP mobility including all the 12 IR modes was

established. *Ab initio* computation was applied to obtain the effective Froehlich coupling of each polar vibrational mode, hence its effectiveness in limiting the carrier mobility. This approach is more accurate than a calculation based on a single effective vibrational mode, as it considers all optical phonons and their relative effect on the lattice mobility. In spite of the approximations of isotropic band and elastic collisions, such an approach turns out to be a useful tool for deriving the electrical parameters by fitting experimental transport data. To assess the robustness of the model, experimental Hall data from the literature have been fitted with very satisfactory results.

Details of the approach

This work extends the approach first proposed by Chang and James for tetragonally-bonded crystals (in particular HgI$_2$ [39]) to β-Ga$_2$O$_3$. The total momentum scattering time for the polar interaction of optical phonons and electrons through the overlap of independent POP modes was calculated. First principle calculations [35–37] were used to calculate spherically average coupling coefficients for each POP contribution and, subsequently, to obtain the energy-dependent total momentum relaxation time for the POP scattering, within the RTA, $\tau_{POP}(\varepsilon)$. These data were then introduced in a routine that simultaneously calculates concentration and drift mobility with the same set of free parameters previously described in [19]. The procedure also includes the self-consistent calculation of the Hall scattering factor for the drift-to-Hall data conversion. Besides the total POP scattering, the model includes scattering by ionized (IO) and neutral impurities (NI), as well as non-polar electron–phonon interactions (discussed below). The Brooks–Herring [40] and Erginsoy models [41] were applied for ionized and neutral impurities, respectively, as described in [19]. Free parameters in the fits are the dopant and compensating impurity densities, the thermal ionization energy of donors, the effective deformation potentials for non-polar electron–phonon interaction (both AC and NOP). Fixed parameters were the *scalar* effective electron mass, taken equal to 0.28 m_o [24] and the mass density, of value 5.88 (g cm^{-3}) [42]. The Farvacque [43] correction to the OP momentum scattering time, which is particularly important for wide band gap semiconductors, was also included (in POP and NOP interaction) and its effect on the Hall scattering factor is critically discussed.

A first principle calculation [35–37] was also applied to calculate the global DP scattering rate separately from the POP one. In addition, the former was split in two contributions: interaction with acoustic phonons, and with optical phonons, respectively. The non-polar scattering rates were calculated from the short-range electron–phonon matrix elements that were obtained using a combination of density functional perturbation theory and maximally localized Wannier functions. Details of the calculation can be found in [37]. In order to facilitate analytical fitting of the computed scattering rates, the non-polar scattering rates are classified between acoustic, centrosymmetric (A$_g$) optical, and non-centrosymmetric optical modes.

Polar optical phonon momentum scattering time

The approach of Chang and James [39] describes the carrier-phonon scattering for non-cubic crystals due to all possible phonon modes and, in particular, leads to the POP carrier mobility through a spherical average of angle-dependent coupling constants, which are defined in order to describe non-isotropic polar electron–phonon interaction. The resulting isotropic momentum scattering times have the same energy dependence normally applied to cubic crystals [44], but differ from the latter by multiplicative coefficients, dependent on the effective charge associated to each POP mode.

It is to be said that Chang and James's approach can be applied to β-Ga$_2$O$_3$, thanks to the nearly spherical CB (nearly isotropic electron effective masses) and negligible mobility anisotropy as mentioned in the introduction. Dispersion relations of all the vibrational modes of β-Ga$_2$O$_3$ were derived from first principles, and the anisotropic scattering probabilities $W_j(\mathbf{k})$ for each IR active mode j were calculated at $T = 300$ K [35–37] and then spherically averaged over the Brillouin zone. After averaging, however, the information on the anisotropy of the LO–TO split is lost. The relative scattering efficiency of each different POP mode was obtained by fitting the relative $W_j(\varepsilon)$ curve with the formula [39, 44]:

$$W_{j,\mathrm{POP}}(\mathcal{E}) = \frac{\overline{C_j^2}}{2\pi\rho\hbar\overline{\omega}_j v_\mathcal{E}} \left\{ n(\overline{\omega}_j)\sinh^{-1}\left(\sqrt{\frac{\mathcal{E}}{\hbar\overline{\omega}_j}}\right) + [n(\overline{\omega}_j)+1]\sinh^{-1}\left(\sqrt{\frac{\mathcal{E}}{\hbar}-1}\right)_{\hbar\overline{\omega}_j} \right\}. \quad (1)$$

Here, ε is the carrier energy, $\hbar$ is the reduced Planck constant, ρ the mass density, $v_\mathcal{E} = \sqrt{2\mathcal{E}/m_e}$, m_e being the *scalar* electron effective mass; $n(\omega_j) = (e^{\hbar\omega_j/KT} - 1)^{-1}$ is the population of phonon of energy $\hbar\omega_j$.

Free parameters of each fit were: the $\overline{C}_j$ coefficient of mode j and the averaged frequency of the optical phonon $\overline{\omega}_j$. The $\overline{C}_j$ coefficients so obtained have the same meaning of the spherically averaged coupling constants defined by Chang and James [39]. The coupling coefficient of each infra-red active mode is related to an *averaged value* of the Callen effective charge associated to such vibrational mode. The first principle scattering rates were calculated using the Vogl method [45]. The net dipole oscillation for a given mode is computed from the tensor product of the Born effective charge matrix and the displacement patterns. The electron–POP matrix element for a given phonon wave-vector is proportional to the projection of this dipole moment along the wave-vector direction. The matrix elements are used in the Fermi–Golden rule to obtain the corresponding scattering rates which are fitted on equation (1) to get the average frequencies $\overline{\omega}_j$ and the coupling parameters $\overline{\overline{C}}_j$. It is important to mention here that the fitted phonon energies do not represent the existence of a mode at those energies. They can be considered as a spherical average of the LO mode energy, as the LO mode energy is strongly dependent on the direction of the phonon wave-vector.

Figure 1 shows the computed $W_j(\varepsilon)$ data and the fitting curves giving the $\overline{C}_j$ coefficients listed in table 1, along with the optimal frequency of each mode and symmetry of the IR active mode. The coupling coefficient and the optimal frequency of each mode were then used to calculate the relative momentum scattering time, from [39]:

$$\frac{1}{\tau_{j,\mathrm{POP}}(\mathcal{E})} = \frac{\overline{C}_j^2}{4\pi\rho\hbar\overline{\omega}_j v_\varepsilon} \left\{ n(\overline{\omega}_j)B^+\left[\sqrt{1 + \frac{\hbar\overline{\omega}_j}{\mathcal{E}}}\right.\right.$$
$$\left. - \frac{\hbar\overline{\omega}_j}{\mathcal{E}}\sinh^{-1}\left(\sqrt{\frac{\mathcal{E}}{\hbar\overline{\omega}_j}}\right)\right] + [n(\overline{\omega}_j)+1]B^-$$
$$\left. \times \left[\sqrt{1 - \frac{\hbar\overline{\omega}_j}{\mathcal{E}}} + \frac{\hbar\overline{\omega}_j}{\mathcal{E}}\sinh^{-1}\left(\sqrt{\frac{\mathcal{E}}{\hbar\overline{\omega}_j}-1}\right)\right]_{\mathcal{E} \geqslant \hbar\overline{\omega}_j} \right\}, \quad (2)$$

where the symbols maintain the meaning described above. Here the factors $B^\pm$ represents the Farvacque correction [43], given by:

$$B^\pm = \pm\frac{f_0(\mathcal{E} \pm \hbar\overline{\omega}_j) - f_0(\mathcal{E})}{\hbar\overline{\omega}_j(\partial f_0/\partial\mathcal{E})}. \quad (3)$$

Such a correction was proposed by Farvacque for each OP scattering mechanism, polar and non-polar, to partially redeem the assumption of elastic scattering required by RTA, indeed rather coarse for OP scattering mechanisms, especially if the energy of the involved phonons is high, as it may occur in wide band gap semiconductors. Considering a single phonon and fixed temperature, the Farvacque correction is different in the process of creation or annihilation of the OP. If energy is transferred from annihilated phonons to electrons, the latter become faster, which is equivalent to having lower collision probability. The final effect is that the momentum scattering *rate* decreases with respect to bare elastic approximation. The opposite occurs when optical phonons are created by highly energetic electrons (see insert of figure 2(b)). Both these effects are enhanced as the temperature decreases, because, according to equation (3), an inelastic process induces a stronger change on the electron distribution function with respect to equilibrium. The final effect of the Farvacque correction on the mobility depends on proper energy averaging (see e.g. [19]) of the momentum scattering *time* and results in an increased mobility. Clearly, the higher the phonon energy the higher the mobility upwards correction. Generally speaking, the Farvacque corrections depends on three factors: temperature, mean carrier energy and distribution of electronic states. Each time the difference between phonon energy and mean carrier energy increases, the inelastic scattering becomes more significant and the Farvacque correction is heavier.

Considering several phonons, as in the present work, the total POP momentum scattering rate is obtained from the overlap of all the $1/\tau_{j,\mathrm{POP}}(\varepsilon)$ POP contributions: this is plotted versus energy, at fixed temperatures in figure 2, either including (F-POP) or excluding (s-POP) the Farvacque correction. The corresponding drift-mobilities obtained from
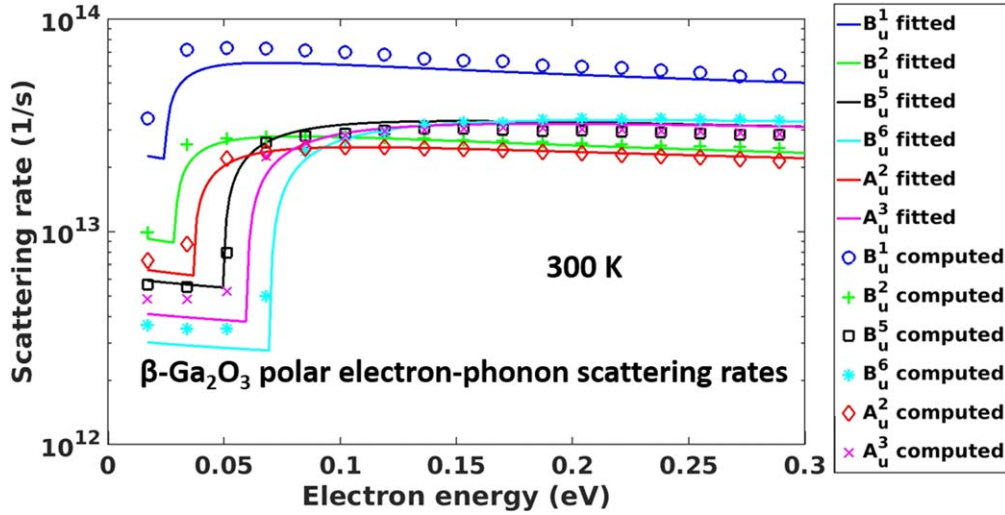
Figure 1. Symbols: averaged $W_j(\varepsilon)$ scattering rates for 6 of the 12 modes with higher scattering rates, obtained by first principle calculations: the anisotropic scattering rates were spherically averaged over the Brillouin zone, which resulted in losing the information on anisotropic LO–TO splitting (see text); lines: fitting curves with equation (1). The sharp increase of the data as the energy increases is due to the process of phonon creation.

Table 1. Averaged coupling constants obtained by fitting the data of figure 1 with equation (1).

Mode	$\overline{\omega}_j$ (eV) (fitted)	$\overline{C}_j$ (eV Å^{-2})
B_u (1)	0.025	2.0
B_u (2)	0.029	1.6
B_u (3)	0.035	0.5
B_u (4)	0.043	1.15
B_u (5)	0.050	3.2
B_u (6)	0.070	4.5
B_u (7)	0.080	3.1
B_u (8)	0.090	3.2
A_u (1)	0.014	0.15
A_u (2)	0.037	2.0
A_u (3)	0.060	3.8
A_u (4)	0.081	3.0

these momentum scattering rates are plotted versus temperature in figure 3.

For comparison, in the figure we also plotted the NOP drift mobility obtained in [19]. The temperature dependence for the set of curves is very similar, although both POP mobility curves are situated a bit under the NOP curve [19]. Furthermore, the F-POP curve is slightly above the s-POP one in the entire temperature range.

It is worth noting that the F-POP and NOP curves are in good agreement also with the POP curve reported in [38], based on the single phonon energy of 44 meV, making us confident that the POP mobility trend indicated by the set of curves is reliable. However, although the single POP mobility curves of figure 3 are similar, the energy dependences of the corresponding momentum scattering times are different. Therefore, they differently influence the calculation of the total momentum scattering time, and the resulting total mobility and Hall scattering factor [19]. From this point of

view, it is important to determine the momentum scattering time as accurately as possible.

Anyway, the observed agreement supports the validity of the RTA approach proposed in this work, and enables its extension to other semiconductors with nearly isotropic effective mass and multiple PO vibrational modes. The validity of the first principle calculations of [35–37] is also indirectly confirmed.

Deformation potential momentum scattering times: AC

Although it plays a minor role, DP electron–phonon interaction is active; therefore, it cannot be neglected in the transport model. First principle calculations [35–37] permitted to compute separately the scattering rates of acoustic and optical phonons.

The calculated scattering rate $W_{AC}(\varepsilon)$ for acoustic phonons obtained by first principle was then fitted by the following standard relation in elastic and equipartition energy approximation [44] to estimate the AC deformation potential, i.e.

$$W_{AC}(\mathcal{E}) = \frac{\sqrt{2}\, m_e^{3/2} k_B T E_{ac}^2}{\pi \hbar^4 \rho v_{\parallel}^2} \mathcal{E}^{1/2}. \tag{4}$$

Figure 4(a) reports the calculated $W_{AC}(\varepsilon)$ together with the fitting curve. The estimated deformation potential was $E_{ac} = 16.6$ eV. The fitting curve closely approaches the calculated scattering rate $W_{AC}(\varepsilon)$ up to energy of about 0.8 eV, thus covering the expected mean energy of carriers in the temperature range of real experimental measurements. Therefore, it is assumed to be a reliable evaluation of the AC deformation potential. In the fitting routine for low-doping samples, we fixed the AC deformation potential at 16.6 eV, whereas we left it as free for samples with higher doping levels. The AC momentum scattering time was taken
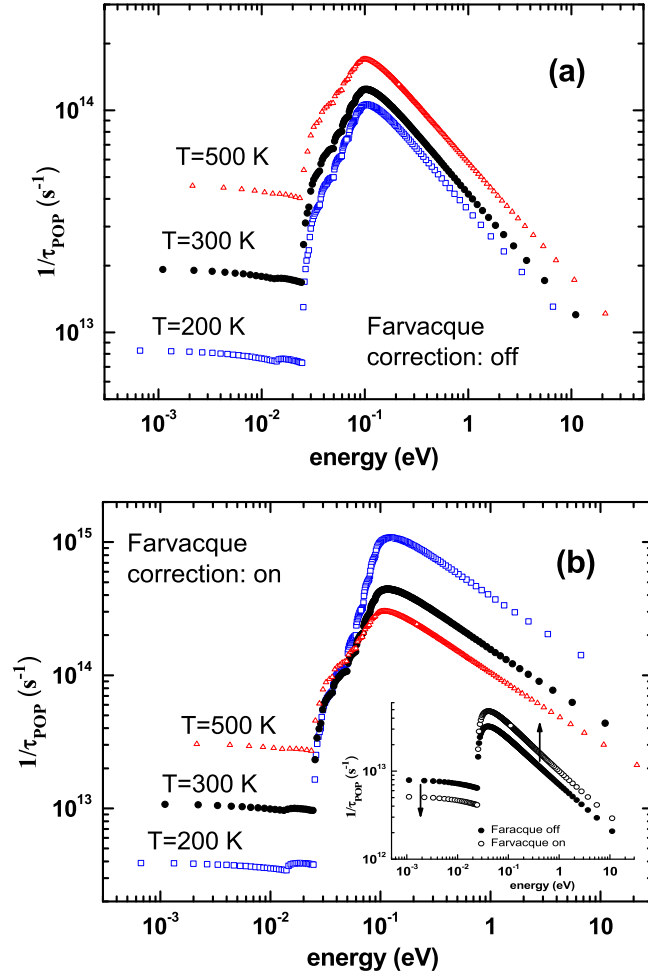
Figure 2. Total POP momentum scattering rate (in RTA) versus energy, obtained from the overlap of all the contributions due to IR active modes, and calculated at three different lattice temperatures. Open triangles: $T = 500$ K; full circles: $T = 300$ K; open squares: $T = 200$ K. (a) Farvacque correction excluded. (b) Farvacque correction included. Notice that the momentum scattering rate, calculated in RTA, is different from the physical scattering rate: Farvacque correction is providing an effective momentum scattering rate in which the crude RTA assumption of elastic scattering for electron–OP interaction is partially adjusted (see text). The insert shows the effect of the Farvacque correction on the POP momentum scattering rate for electron interaction with a single phonon of 25 meV, at $T = 300$ K: the arrows help to understand the effect of the correction (full circles: correction off; empty circles: correction on).

coincident with equation (4), the collision probability being isotropic.

Deformation potential momentum scattering times: NOP

Concerning the NOP contributions, figure 4(b) gives the energy dependence of the overall NOP scattering rate due to all vibrational modes (open symbols) in log–log scale. In the same figure, the contributions due to all centrosymmetric (A_g)
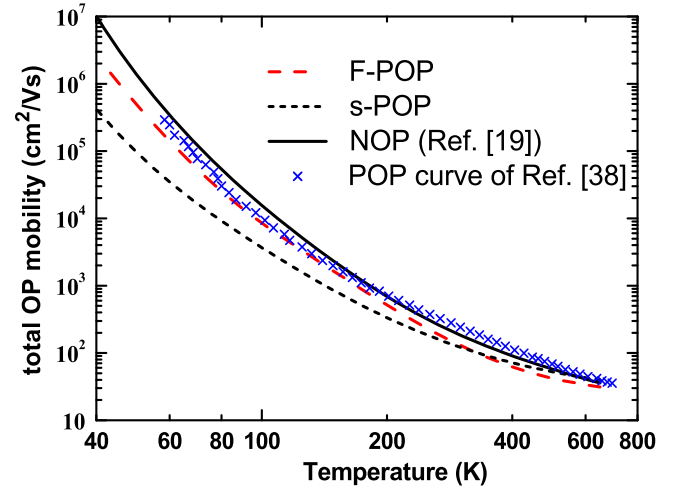

Figure 3. Total POP mobility versus temperature, obtained from the overlap of all the POP contributions, with (dash) or without (short dash) Farvacque correction, compared to the single NOP effective mobility (continuous line) given in [19] and to the effective POP curve (crosses) given in [38].

optical, and non-centrosymmetric optical modes are plotted separately. The calculated scattering rates seem to mix contributions of zero and first order NOP interaction, excluding the prevalence of an effective optical vibrational mode in the non-polar interaction. In particular, for $\mathcal{E} \gg \hbar\omega_{nop}$, where $\hbar\omega_{nop}$ is the energy of the optical phonon involved, a $\sqrt{\mathcal{E}}$ or a $\mathcal{E}^{1.5}$ energy dependence of the scattering rate is expected for the zero (see equation (5)) or the first order NOP interaction, respectively [39, 44]

$$W_{\text{NOP-0}}(\mathcal{E}) = \frac{\sqrt{2}\,E_{nop}^2\,m_e^{3/2}}{4\pi\rho\hbar^3\omega_{nop}}\{n(\omega_{nop})\sqrt{\mathcal{E} + \hbar\omega_{nop}}$$
$$+ [[n(\omega_{nop}) + 1]\sqrt{\mathcal{E} - \hbar\omega_{nop}}]_{E \geqslant \hbar\omega_{nop}}\}. \quad (5)$$

Here E_{nop} and $\hbar\omega_{nop}$ are the NOP deformation potential and the energy of the optical phonon involved in the interaction, respectively [39, 44]. The same conclusion is obtained if the NOP scattering rate is calculated including only the 10 A_g centrosymmetric OP modes, (full circles in figure 4(b)), or the non-centrosymmetric ones (full squares in figure 4(b)), notwithstanding the different symmetries of the two sets of phonons.

Considering all this, for simplicity, in the RTA calculation the NOP scattering was handled through a momentum scattering time for a *single* zero-order non-polar interaction (NOP-0), see [44], including the Farvacque correction [43]:

$$\frac{1}{\tau_{\text{NOP}}(\mathcal{E})} = \frac{E_{nop}^2\,m_e^{3/2}}{\sqrt{2}\,\pi\rho\hbar^3\omega_{nop}}G(\mathcal{E}).$$

$$G(\mathcal{E}) = n(\omega_{nop})B^+\sqrt{\mathcal{E} + \hbar\omega_{nop}} + \{[n(\omega_{nop}) + 1]$$
$$\times B^-\sqrt{\mathcal{E} - \hbar\omega_{nop}}\}_{\mathcal{E} \geqslant \hbar\omega_{nop}}. \quad (6)$$
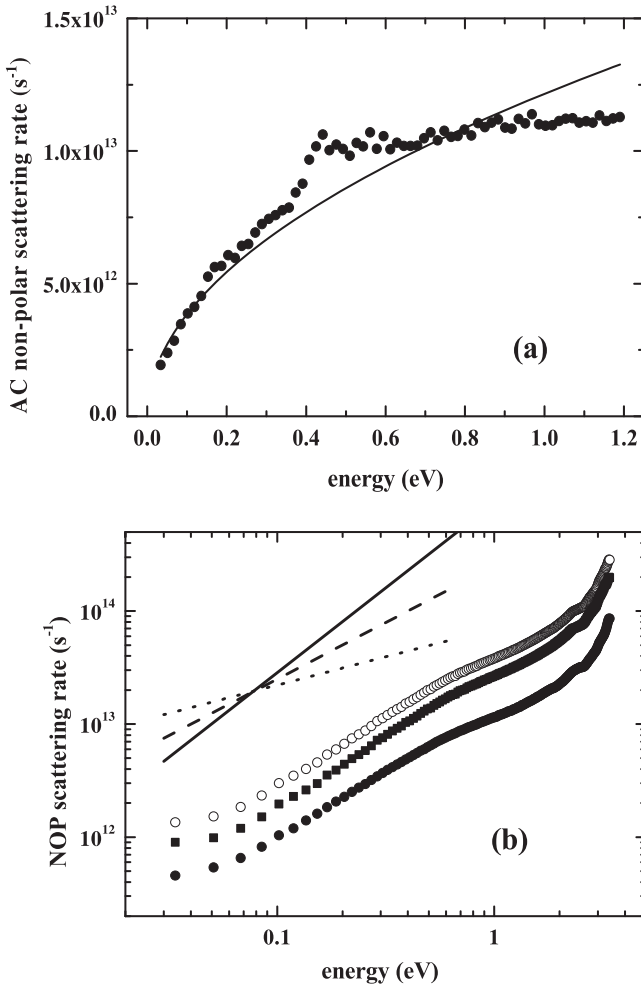
Figure 4. Scattering rates due to non-polar electron–phonon coupling: (a) acoustic phonon, symbols indicate the data obtained from first principle calculations [35–37], whereas the line indicates the fitting of the curve by equation (4) to derive the AC deformation potential; (b) overall contribution of all optical phonons (empty circles); of the 10 A_g centrosymmetric optical phonons (full circles); and the remaining 17 optical phonons (full squares). Lines indicates the square root (dotted line), linear (dashed line) and $\mathcal{E}^{1.5}$ (continuous line) energy dependences.

Both the effective deformation potential E_{nop} and the effective phonon energy $\hbar\omega_{\mathrm{nop}}$ were thus kept as adjustable phenomenological parameters.

Analytical approach applied to analysis of experimental data

When Hall data of samples with different doping levels are analyzed by the methodology described above, but with no Farvacque correction, a good fit is obtained only for low-doped samples (up to about $1 \times 10^{17}\,\mathrm{cm}^{-3}$). As the doping level increases above $10^{17}\,\mathrm{cm}^{-3}$, the calculated mobility resulted appreciably lower than the experimental mobility, even if the non-polar interaction was completely excluded. This is due to the increasing effectiveness of the ionized impurity scattering at the higher temperatures, which can
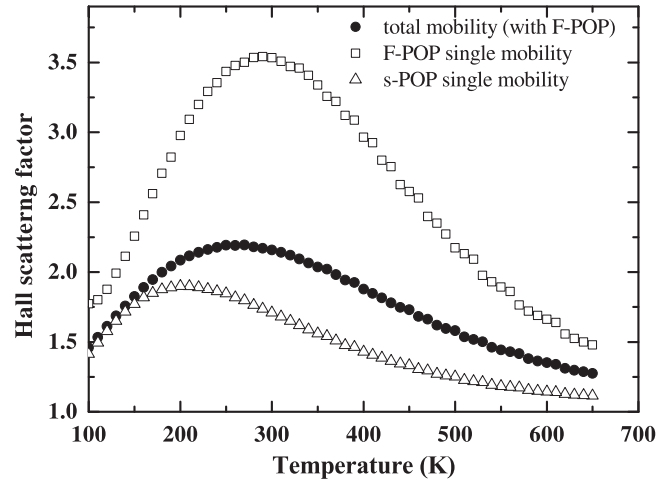

Figure 5. Hall scattering factor due to F-POP full scattering (open squares), and to s-POP full scattering (open triangles) compared to the total r_{H} curve (full symbols) derived from the fitting of sample Irmscher#12 (free parameters of table 2).

dominate over the phonon scattering. On the other hand, fitting of the entire set of experimental data was possible when the total POP momentum scattering time was corrected by Farvacque factors.

We observe that the action of the Farvacque factor, in the present analysis, is double: first, it enhances the absolute drift mobility values, as expected. Secondly, the Hall scattering factor, generally higher than unity, increases the drift mobility. Figure 5 shows that the Farvacque correction indeed enhances r_{H}. As a result, the calculated Hall mobility is greater for the F-POP momentum scattering time than for the simple POP. In this regards, it is worth noting that the maximum Hall factor associated to the standard POP mobility (for a single vibrational mode) reaches 1.9 without Farvacque correction, but goes above 3 after correction.

Such enhancement effect by Farvacque factor is crucial in order to fit the experimental lattice mobility, in particular at higher doping levels, where the ionized impurity scattering becomes competitive with the phonon scattering and significantly decreases the computed mobility. Actually, the progressive apparent reduction of the non-polar scattering contributions, both AC and NPO, would seem to improve the accuracy of the experimental data fitting. However, this is a non-physical result, which suggests a slight overestimation of the total F-POP momentum scattering rate, i.e. the total F-POP mobility is probably underestimated.

The analytic procedure was applied to the analysis of Hall mobility and Hall density data from the literature, in particular from [22, 28]. The calculated Hall curves are reported in figures 6(a) and (b); the fitting is limited to the temperature range where the effects of the impurity band conduction are negligible. The Hall factors self-consistently obtained are reported in figure 6(c). The values of the free parameters entering in the iterative calculation are given in table 2. Here, N_{D}, N_{A}, $N_{\mathrm{A}}/N_{\mathrm{D}}$ and E_{D} indicate the donor and acceptor density, the compensation ratio and the thermal ionization energy of the donors, respectively. Note that the
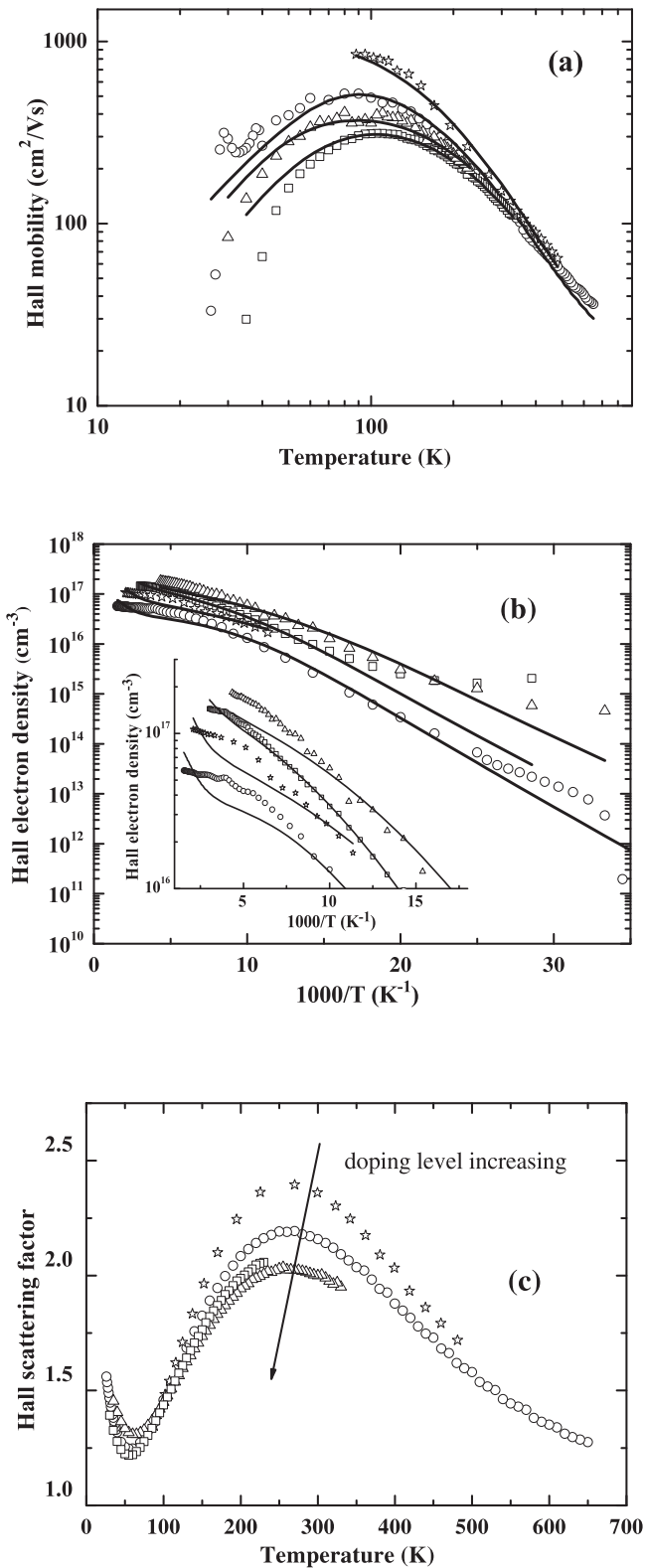
Figure 6. Temperature dependent Hall mobility data (a) and Hall density data (b); insert: detail of (b). In the figures the symbols represent experimental data: stars Oishi#1 [28]; circles Irmscher#12 [22]; squares Irmscher#3 [22]; triangles Irmscher#7 [22]; solid lines are from theory using the free parameters of table 2. (c) Hall scattering factor for the same samples represented by same symbols as in (b). Here, the arrow is a guide for the reader; the doping level of the samples is given in table 2.

role of the DP contributions tends to decrease at higher doping level, as pointed out above. In the lowest doped sample, a value higher than the typical one of about 10^8 eV cm^{-1} was obtained for the NOP deformation potential. This result must be taken with some precaution because such a parameter is here purely phenomenological.

Although the Hall data of the two most conductive samples resulted compatible with a weak DP scattering, the quality of the fit did not vary appreciably when the DP contribution was neglected.

It is apparent, that the experimental mobility data are well fitted by the theoretical curves in the range of temperature where the transport takes place through the CB extended states, which backs the approach followed for calculation of the F-POP mobility. The F-POP mechanism results to dominate the lattice mobility as proposed in [35]. It should be noted that the calculated Hall densities show an unphysical effect, namely an inflection correlated with the total Hall scattering factor. A similar, weaker, inflection also appears if the Farvacque correction is not applied, which again indicates a slight overestimation of the POP momentum scattering rate. The values of the parameters obtained from the best fitting however seem to be physically meaningful, because the distortion of the theoretical curve is limited to a narrow T range. These parameters are consistent, within 10% of uncertainty, with those estimated in [19].

In view of the comparable accuracy of van der Pauw measurements, owing to the finite dimensions of the contacts [46], we are confident that the present analytical procedure may provide a reliable interpretation of the actual scattering phenomena in β-Ga$_2$O$_3$. The reliability of the estimated donor and acceptor densities is expected to further increase if a wider temperature range is investigated, up to the carrier freezing region.

In samples doped at higher levels, of the order of 10^{18} cm^{-3} [29], the electron transport is strongly affected by impurity band conduction, thus hindering the CB transport also above RT. We in turn expect that the Hall data of highly-doped samples cannot be fitted correctly by present model, also considering that screening effects could influence the F-POP scattering time leading to different $\overline{C_j}$ coefficients.

As a final point, we should note that the estimated compensation ratios are generally lower than previously reported in [23, 28]. The discrepancy is particularly high between the N_A/N_D ratio given by Oishi *et al* (0.19, see [28]) and the present recalculation. However, we notice that in the model of Oishi *et al* the lattice mobility was described by a single phonon POP momentum scattering time, without any correction for the Hall scattering factor, and that no OP energy was provided. More information about their experimental measurements and the way they estimated the compensation ratio would be very helpful in order to understand the reasons behind discrepancy. However, it is to be underlined that the higher mobility and higher Hall electron density in [28] than in sample Irmscher#12 [22] are actually compatible with a significantly lower compensation ratio.

Table 2. Parameters estimated from the best fits of experimental data taken from the literature. Note that both the effective deformation potential E_{nop} and the effective phonon energy $\hbar\omega_{nop}$ were kept as adjustable phenomenological parameters, therefore their values must be read with some caution.

Sample	N_D (cm^{-3})	N_A (cm^{-3})	N_A/N_D	E_D (eV)	E_{ac} (eV)	E_{nop} (eV cm^{-1})	$\hbar\omega_{nop}$ (eV)
Oishi#1 [28]	2.5×10^{17}	2.5×10^{15}	0.01	0.034	16.6	15.4×10^8	0.030
Irmscher#12 [22]	1.3×10^{17}	3.3×10^{16}	0.25	0.029	16.6	8.5×10^8	0.014
Irmscher#3 [22]	5.2×10^{17}	6.8×10^{16}	0.13	0.027	2.13	4.6×10^8	0.030
Irmscher#7 [22]	5.75×10^{17}	5.17×10^{15}	0.01	0.024	2	4×10^8	0.090

An attempt to use the compensation ratio of 0.19 given by Oishi *et al* results in a discrepancy between experimental and theoretical Hall mobility only below $T \approx 150$ K and without significant variations from the phonon parameters of table 2. This means that, up to compensation ratios of 0.19, the high temperature mobility data of Oishi *et al* should not be affected by impurity scattering; therefore, the fitting of such a set of data strongly supports the reliability of the analytical approach proposed in the present paper.

Conclusions

A method to calculate the energy-dependent momentum scattering time for electron-optical phonon interaction in β-Ga$_2$O$_3$ is presented. The method is developed in the frame of RTA and takes into account the contributions of the 12 IR active modes. First principle calculations were applied to derive spherically averaged coupling coefficients for the polar optical phonon interaction, to weight the vibrational optical modes and to derive their corresponding momentum scattering rates. This model takes into account POP, AC and NOP deformation potentials, and allows for a satisfactory fit of experimental Hall data of samples with different carrier concentrations, provided that the Farvacque correction is included. The role of such correction as well as of the Hall scattering factor, self-consistently calculated in the fitting routine for the drift-to-Hall data conversion, are critically discussed. In this way, we arrived to set the range of application of the proposed approach.

In conclusion, this analysis represents the first successful RTA-based fitting of transport data of β-Ga$_2$O$_3$ that takes into account the multiplicity of POP phonons of the monoclinic lattice; therefore, it is more complete than any other approach reported so far. In addition, we suggest that the proposed approach can be generally applied to the analyses of transport data in semiconducting materials having a multiplicity of optical phonons, provided that CB can be treated as isotropic.

Acknowledgments

ORCID iDs

A Parisini ⬤ https://orcid.org/0000-0003-4212-5074
K Ghosh ⬤ https://orcid.org/0000-0002-1175-8138

References

[1] Higashiwaki M, Sasaki K, Kuramata A, Masui T and Yamakoshi S 2014 *Phys. Status Solidi Appl. Mater. Sci.* **211** 21
[2] Hwang W S *et al* 2014 *Appl. Phys. Lett.* **104** 249902
[3] Nakagomi S, Momo T, Takahashi S and Kokubun Y 2013 *Appl. Phys. Lett.* **103** 72105
[4] Oshima T, Okuno T, Arai N, Suzuki N, Hino H and Fujita S 2009 *Japan. J. Appl. Phys.* **48** 011605
[5] Liu X Z, Guo P, Sheng T, Qian L X, Zhang W L and Li Y R 2016 *Opt. Mater.* **51** 203
[6] Nakagomi S, Sai T and Kokubun Y 2013 *Sensors Actuators* B **187** 413
[7] Bartic M, Baban C-I, Suzuki H, Ogita M and Isai M 2007 *J. Am. Ceram. Soc.* **90** 2879
[8] Higashiwaki M, Sasaki K, Murakami H, Kumagai Y, Koukitu A, Kuramata A, Masui T and Yamakoshi S 2016 *Semicond. Sci.Technol.* **31** 034001
[9] Pearton S J, Yang J, Cary P H, Ren F, Kim J, Tadjer M J and Mastro M A 2018 *Appl. Phys. Rev.* **5** 011301
[10] Tsao J Y *et al* 2018 *Adv. Electron. Mater.* **4** 1600501
[11] Stepanov S I, Nikolaev V I, Bougrov V E and Romanov A E 2016 *Rev. Adv. Mater. Sci.* **44** 63
[12] Higashiwaki M, Sasaki K, Kuramata A, Masui T and Yamakoshi S 2014 *Phys. Status Solidi* a **211** 21
[13] Ueda N, Hosono H, Waseda R and Kawazoe H 1997 *Appl. Phys. Lett.* **71** 933
[14] Ricci F, Boschi F, Baraldi A, Filippetti A, Higashiwaki M, Kuramata A, Fiorentini V and Fornari R 2016 *J. Phys.: Condens. Matter* **28** 224005
[15] Guo Z, Verma A, Wu X, Sun F, Hickman A, Masui T, Kuramata A, Higashiwaki M, Jena D and Luo T 2015 *Appl. Phys. Lett.* **106** 111909
[16] Santia M D, Tandon N and Albrecht J D 2015 *Appl. Phys. Lett.* **107** 041907
Santia M D, Tandon N and Albrecht J D 2016 *Appl. Phys. Lett.* **109** 049901 (erratum)
[17] Liu B, Gu M and Liu X 2007 *Appl. Phys. Lett.* **91** 172102
[18] Onuma T, Fujioka S, Yamaguchi T, Itoh Y, Higashiwaki M, Sasaki K, Masui T and Honda T 2014 *J. Cryst. Growth* **401** 330
[19] Parisini A and Fornari R 2016 *Semicond. Sci. Technol.* **31** 035023
[20] Smith A C, Janak J F and Adler R B 1967 *Electronic Conduction in Solids* (New York: McGraw-Hill)
[21] Bhagavantam S 1966 *Crystal Symmetry and Physical Properties* (London, New York: Academic)
[22] Irmscher K, Galazka Z, Pietsch M, Uecker R and Fornari R 2011 *J. Appl. Phys.* **110** 063720

[23] Kang Y, Krishnaswamy K, Peelaers H and Van de Walle C G 2017 *J. Phys.: Condens. Matter* **29** 234001

[24] Varley J B, Weber J R, Janotti A and Van de Walle C G 2010 *Appl. Phys. Lett.* **97** 142106

[25] Villora E G, Shimamura K, Yoshikawa Y, Aoki K and Ichinose N 2004 *J. Crystal Growth* **270** 420

[26] Wong M H, Sasaki K, Kuramata A, Yamakoshi S and Higashiwaki M 2016 *Japan. J. Appl. Phys.* **55** 1202B9

[27] Bierwagen O, Pomraenke R, Eilers S and Masselink W T 2004 *Phys. Rev.* B **70** 165307

[28] Oishi T, Koga Y, Harada K and Kasu M 2015 *Appl. Phys. Express* **8** 031101

[29] Kabilova Z, Kurdak C and Peterson R L 2017 *Proc. 2nd Int. Workshop on Ga₂O₃ and Related Materials, IWGO2017 (Parma, Italy, 12–15 September)*

[30] Oishi T, Harada K, Koga Y and Kasu M 2016 *Japan. J. Appl. Phys.* **55** 030305

[31] Moser N *et al* 2017 *IEEE Electron Device Lett.* **38** 775

[32] Rafique S, Han L, Neal A T, Mou S, Boeckl J and Zhao H 2017 *Phys. Status Solidi* a **215** 1700467

[33] Sasaki K, Kuramata A, Masui T, Villora E G, Shimamura K and Yamakoshi S 2012 *Appl. Phys. Express* **5** 035502

[34] Baldini M, Albrecht M, Fiedler A, Irmscher K, Schewski R and Wagner G 2017 *ECS J. Solid State Sci. Technol.* **6** Q3040

[35] Ghosh K and Singisetti U 2016 *Appl. Phys. Lett.* **109** 072102

[36] Ghosh K and Singisetti U 2017 *J. Mater. Res.* **32** 4142

[37] Ghosh K and Singisetti U 2017 *J. Appl. Phys.* **122** 035702

[38] Ma N, Tanen N, Verma A, Guo Z, Luo T, Xing (Grace) H and Jena D 2016 *Appl. Phys. Lett.* **109** 212101

[39] Chang Y C and James R B 1996 *Phys. Rev.* B **53** 14200

[40] Chattopadhyay D and Queisser H J 1981 *Rev. Mod. Phys.* **53** 745

[41] Erginsoy C 1950 *Phys. Rev.* **79** 1013

[42] Weast R C, Lide D R and Beyer W H 1986–1987 *CRC Handbook of Chemistry and Physics* 67th edn (Boca Raton, FL: CRC Press) p B-92

[43] Farvacque J L 2000 *Phys. Rev.* B **62** 2536

[44] Ridley B K 1982 *Quantum Processes in Semiconductors* (Oxford: Clarendon) p 128

[45] Verdi C and Giustino F 2015 *Phys. Rev. Lett.* **115** 176401

[46] Chwang R, Smith B J and Crowell C R 1974 *Solid State Electron* **17** 1217